The sequences appended to the amyloid core region of the HET-s prion protein determine higher-order aggregate organization in vivo

Axelle Balguerie[1], Suzana Dos Reis[1], Bénédicte Coulary-Salin[1], Stéphane Chaignepain[1,2], Martine Sabourin[1], Jean-Marie Schmitter[1,2] and Sven J. Saupe[1,*]

[1]Laboratoire de Génétique Moléculaire des Champignons, Institut de Biochimie et de Génétique Cellulaires, UMR 5095 CNRS/Université de Bordeaux 2, 1 rue Camille St Saëns, 33077 Bordeaux, France
[2]Institut Européen de Chimie et Biologie CNRS FRE 2247 16, Avenue Pey Berland 33607 Pessac Cedex, France
*Author for correspondence (e-mail: sven.saupe@ibgc.u-bordeaux2.fr)

Accepted 22 January 2004
Journal of Cell Science 117, 2599-2610 Published by The Company of Biologists 2004
doi:10.1242/jcs.01116

Summary

The [Het-s] prion of the fungus *Podospora anserina* propagates as a self-perpetuating amyloid form of the HET-s protein. This protein triggers a cell death reaction termed heterokaryon incompatibility when interacting with the HET-S protein, an allelic variant of HET-s. HET-s displays two distinct domains, a N-terminal globular domain and a C-terminal unstructured prion-forming domain (residues 218-289). Here, we describe the characterization of HET-s(157-289), a truncated form of HET-s bearing an extensive deletion in the globular domain but retaining full activity in incompatibility and prion propagation. In vitro, HET-s(157-289) polymerizes into amyloid fibers displaying the same core region as full-length HET-s fibers. We have shown previously that fusions of green fluorescent protein (GFP) with HET-s or HET-s(218-289) form dot-like aggregates in vivo upon transition to the prion state. By contrast, a HET-s(157-289)/GFP fusion protein forms elongated fibrillar aggregates in vivo. Such elongated aggregates can reach up to 150 μm in length. The in vivo dynamics of these organized structures is analysed by time lapse microscopy. We find that the large elongate structures grow by lateral association of shorter fibrillar aggregates. When co-expressed with HET-s(157-289), full-length HET-s and HET-s(218-289) can be incorporated into such elongated aggregates. Together, our data indicate that HET-s(157-289) aggregates can adopt an organized higher-order structure in vivo and that the ability to adopt this supramolecular organization is conferred by the sequences appended to the amyloid core region.

Movies available online

Key words: Prion, Amyloid, Cell death, Incompatibility, Fungi

Introduction

Prions are infectious proteins that are able to propagate an altered conformational state (Prusiner, 1982). The term was coined to designate the infectious elements responsible for spongiform encephalopathies in mammals, a group of fatal neurodegenerative affections that include Creutzfeldt-Jacob disease in humans and mad-cow disease in cattle (Prusiner, 1998). In the protein-only model, these diseases are caused by the infectious propagation of an altered conformation of the PrP protein. Prion diseases are related to a large group of human diseases, all characterized by the systemic or intracerebral deposition of fibrillar β-sheet-rich protein aggregates termed amyloids (Taylor et al., 2002). However, unlike prion diseases, others amyloid diseases (such as Alzheimer's and Parkinson's diseases) do not display an infectious character. The prion phenomenon is not limited to mammalian PrP. Proteins that can propagate an altered conformation have also been discovered in lower eukaryotes, including yeast (Wickner, 1994; Uptain and Lindquist, 2002) and the filamentous fungus *Podospora anserina* (Coustou et al., 1997).

The HET-s prion protein of the filamentous ascomycete *P. anserina* is involved in a genetically controlled programmed cell death phenomenon termed heterokaryon incompatibility. Heterokaryon incompatibility is very common in filamentous fungi and occurs when two fungal strains of unlike genotype fuse (for a review, see Glass and Kaneko, 2003). Heterokaryon incompatibility constitutes a self versus non-self discrimination system preventing cytoplasmic mixing between genetically unlike individuals. Cell death by incompatibility is triggered by genetic differences at particular loci, termed *het* loci. The *het-s* locus is one of ten heterokaryon incompatibility loci of *P. anserina*. Two distinct alleles of this gene have been described and termed *het-s* and *het-S* (Rizet, 1952; Beisson-Schecroun, 1962; Turcq et al., 1990). The *het-s* and *het-S* alleles encode cytosolic proteins of 289 amino acids that differ by 13 residues and display no homologs of known function in other species (Turcq et al., 1991; Coustou-Linares et al., 2001). The HET-s protein can (unlike HET-S) exist in both a normal form and an infectious prion form (Coustou et al., 1997). Strains carrying the protein in its normal form are designated [Het-s*], whereas strains carrying the prion form of HET-s are designated [Het-s]. It is the prion form of HET-s that is active in heterokaryon incompatibility. A fusion between a

[Het-s*] and a [Het-S] strain is normal, whereas a fusion between a [Het-s] (prion-infected) strain and [Het-S] is lethal. In other words, the [Het-s] prion is not detrimental per se but only becomes toxic when interacting with HET-S. The [Het-s] prion can appear spontaneously at a low frequency and is readily transmitted from one strain to another by simple contact (Beisson-Schecroun, 1962).

Transition to the [Het-s] prion state correlates with conversion of the HET-s protein to an aggregated state (Coustou-Linares et al., 2001). Recombinant HET-s protein forms amyloid fibrils in vitro (Dos Reis et al., 2002). These HET-s amyloid fibers generated in vitro were found to display [Het-s] infectivity when reintroduced into [Het-s*] fungal cells using a biolistic procedure (Maddelein et al., 2002). We have thus proposed that [Het-s] propagates as a self-perpetuating amyloid form of the HET-s protein. We have recently reported that HET-s displays two distinct domains, an N-terminal well-folded, mainly α-helical, domain and a unstructured C-terminal domain (residues 218-289) (Balguerie et al., 2003). This C-terminal flexible tail is essential for prion propagation and incompatibility in vivo and amyloid formation in vitro. When fused to green fluorescent protein (GFP), the C-terminal domain of HET-s is able to propagate the [Het-s] prion but does not display normal incompatibility function. Hence, whereas the C-terminal prion-forming domain (PFD) alone allows [Het-s] propagation, it is not sufficient to perform the incompatibility function.

Here, we show that a truncated version of HET-s encompassing the 133 C-terminal residues (157-289) retains [Het-s] activity in terms of both prion propagation and incompatibility. We have analysed in vitro and in vivo polymerization of this protein. In contrast to full-length HET-s or the HET-s(218-289) PFD, this functional truncated form polymerizes into very large elongated aggregates in vivo. We use this system to explore the mechanisms that govern higher-order prion protein aggregate organization in vivo.

Materials and Methods

Plasmids

In all *Podospora* vectors, expression of the HET-s constructs was driven by the GPD promoter of *Aspergillus nidulans* (Punt et al., 1988). For construction of the pGPD-het-s(157-289) plasmid, the region encoding the C-terminal part of HET-s (residue 157 to 289) was amplified using the polymerase chain reaction (PCR) (oligonucleotides 5′-ATCCATGGAGAAAATAGTCGA-3′ and 5′-TAAGATCTTTTAGTGATGATGGTGATGGTG-3′) and cloned as a *Nco*I-*Bgl*II fragment into the *Nco*I and *Bam*HI sites of the pAN52.1 vector (Punt et al., 1988). For construction of the pGPD-het-S(157-289) plasmid, the pGPD-het-S vector (Coustou-Linares et al., 2001) was amplified by inverse PCR (oligonucleotides Nco157 5′-CATGCCATGGGCGAGAAAATAGTCGACCAGG-3′ and NcoGPD 5′-CATGCCATGGTGATGTCTGCTCAAGC-3′). The PCR product was digested by *Nco*I and cloned into the *Nco*I site of the pAN52.1 vector (Punt et al., 1988). For construction of the pGPD-het-s(157-289)-GFP plasmid, the 5′ region of the *het-s* ORF allowing expression of HET-s(157-289) peptide was amplified by PCR (oligonucleotides: 5′-CCCTCATGATGGAGAAAATAGTCGACCAGGTC-3′ and 5′-CCCTCATGACATTATCCCAGAACCCCTTAC-3′). The PCR product was cloned as a *Bsp*HI fragment into the *Nco*I site of pAN52.1-GFP vector (Pinan-Lucarre et al., 2003). For construction of the pGPD-het-S(155-289)-GFP plasmid, the *Bgl*II-*Xba*I fragment of the pGSGFP (Coustou-Linares et al., 2001) was introduced into the *Bgl*II and *Xba*I sites of the Litmus 28 vector (Biolabs). The LitmusGSGFP vector was then amplified by inverse PCR (oligonucleotides 5′-CATGCCATGGGCGAGAAAATAGTCGACCAGG and 5′-CATGCCATGGTGATGTCTGCTCAAGC-3′). The PCR product was digested with *Nco*I and circularized by ligation.

For construction of the pET-het-s(157-289) allowing expression of the HET-s(157-289) protein tagged with six histidine residues at the C-terminus, the region coding for the C-terminal part of HET-s was amplified by PCR (oligonucleotides 5′-ATCATATGCTCGAGAAAATAGCGACC-3′ and 5′-ATAAGCTTAGTGATGATGGTGATGGTGATTATCCCAGAACCC-3′), the PCR product was then cloned as a *Nde*I-*Hin*dIII fragment into the pET-21a vector (Novagen).

Prion propagation, incompatibility assays and *Podospora* methods

The *P. anserina* strains used in this study (*het-S*, *het-s* and *Δhet-s*) are isogenic except for the *het-s* locus. In *Δhet-s*, the *het-s* gene has been inactivated by gene replacement (Turcq et al., 1991). In this strain, the promoter region and the 5′ part of the *het-s* gene have been deleted and replaced by the *ura5* marker. The [Het-s*] strains are obtained as the progeny of a *het-S* × *het-s* cross.

Incompatibility phenotypes were determined by performing barrage tests on cornmeal agar medium as previously described (Maddelein et al., 2002). In brief, strains are confronted on solid cornmeal medium and, after 2 days of growth, a characteristic dense line appears in the confrontation region between the two mycelia if strains are incompatible. This dense line termed the ‘barrage’ corresponds to the macroscopic manifestation of the cell death reaction.

[Het-s] prion propagation was assayed as the ability to transmit the [Het-s] prion from a [Het-s]-donor strain to a [Het-s*] prion-free tester strain. To that end, transformants were first confronted to a wild-type [Het-s]-strain and then subcultured twice and confronted with a [Het-s*] prion-free tester strain. The tester strains were then assayed for their [Het-s] status in barrage tests as described here above.

DNA-mediated transformation of *Podospora* strains was performed as described (Bergès and Barreau, 1989). Plasmids were introduced in co-transformation experiments using a 10:1 molar ratio between the plasmid of interest and the pCB1004 vector carrying the *hygR* gene used as selective marker (Carrol et al., 1994). Transforming DNA integrates in the genome mainly by non-homologous recombination, so all transformants display a distinct genetic constitution. Thus, in each experiment, from 12 to 24 individual transformants were analysed.

Protein methods

The histidine-tagged HET-s(157-289) protein was expressed and purified from inclusion bodies under denaturing conditions as previously described for full-length HET-s (Dos Reis et al., 2002). This procedure yielded ~2-4 mg of peptide per liter of culture. The peptide was pure as judged by sodium-dodecyl-sulfate polyacrylamide-gel electrophoreses (SDS-PAGE) followed by Coomassie-Blue staining. To eliminate urea, the peptide was then submitted to gel filtration on Sephadex G-25 using 50 mM Tris-HCl, pH 8, 150 mM NaCl, 1 mM DTT as eluent.

For spontaneous and seeded aggregation assays, protein solutions were incubated at room temperature in 50 mM Tris-HCl pH 8.0, 150 mM NaCl. Protein precipitation was analysed at various time points by centrifuging 50 μl aliquots for 15 minutes at 10,000 ***g***. Supernatant and pellet fractions were analysed by SDS-PAGE followed by Coomassie-Blue staining and protein concentration in the supernatant fractions was measured using the BioRad protein-assay reagent and determining absorbance at 280 nm. For seeding assays, a 25 μM protein solution in 50 mM Tris-HCl pH 8.0, 150 mM NaCl was

inoculated with 2.5 μM aggregated protein. The aggregated protein sample was sonicated briefly before inoculation. Protein precipitation was analysed as described above.

Circular dichroism (CD) spectra were recorded at 20°C using a Jasco 810 spectropolarimeter with a quartz cell of 0.1 cm path length.

For limited proteolysis of HET-s(157-289) with proteinase K, a 30 μM solution of soluble and aggregated HET-s protein was treated for various times at 37°C with 2 μg ml^{-1} proteinase K in 50 mM Tris-HCl pH 8.0, 150 mM NaCl. Reactions were stopped by addition of one volume of SDS-PAGE loading buffer and heated at 100°C for 5 minutes. SDS-PAGE was performed using 16.5% Tricine precast gels (Biorad).

Mass spectrometry of HET-s(157-289) proteinase-K digestion products

A 30 μM solution of aggregated HET-s(157-289) was digested for 40 minutes at 37°C with 2 μg ml^{-1} proteinase K in 50 mM Tris-HCl pH 8.0, 150 mM NaCl. The reaction mixture was centrifuged for 10 minutes at 10,000 ***g*** and the pellet fraction resuspended in H_2O. The matrix-assisted laser desorption ionization (MALDI) mass spectrometer was a Reflex III (Bruker) instrument equipped with a 337 nm laser source. α-Cyano-4-hydroxy-cinnamic acid (Sigma) was used as a matrix [saturated solution in 50% acetonitrinile in 0.1% aqueous trifluoroacetic acid (TFA)]. The dried droplet method was used for sample loading on stainless steel targets. Average masses of proteinase K digestion products were measured in the linear mode using an internal calibration with a mixture of two bovine proteins, insulin (theoretical mass 5734.60 Da) and cytochrome *c* (theoretical mass 12361.09 Da) (Sigma).

Microscopy

For fluorescence microscopy, synthetic medium containing 2% (w/v) agarose was poured as two 10 ml layers of medium. *P. anserina* hyphae were inoculated on this medium and cultivated for 16-24 hours at 26°C. The top layer of the medium was then cut out and the mycelium examined with a Leica DMRXA microscope equipped with a Micromax CCD (Princeton Instruments) controlled by Metamorph 5.06 software (Roper Scientific). The microscope was fitted with a standard FITC filter set (Leica L4) and a Leica PL APO 100× immersion objective.

For time-lapse microscopy, samples were mounted as follows in order to prevent desiccation. A glass slide was overlaid with three pieces of soft PVC of 1 mm thickness (REVOL et SOLNIER, Vaux-en-Velin, France) in which a well of about 15×30 mm was cut. Synthetic medium containing 2% agarose was poured into the well and immediately flattened by covering it with a glass slide. The top slide was removed, leaving a flattened agarose plug. A preculture was grown on cellophane film laid on solid medium for 16-20 hours at 26°C. For inoculation, a square of cellophane film of about 1 cm^2 was cut out from the preculture and laid on the agarose plug. The agarose plug was then overlaid with a coverslide and sealed with Vaseline.

Electron microscopy of fibrils generated in vitro was performed as previously described (Dos Reis et al., 2002). For electron microscopy on hyphae, a modification of the chemical fixation technique described by Chang and Tanaka was used (Chang and Tanaka, 1970). *Podospora* mycelium cultivated on cellophane was fixed for 4 hours in 2.5% glutaraldehyde solution in 0.1 M sodium phosphate buffer, pH 7.2. After several washes, samples were post-fixed overnight at 0°C with 1% OsO_4 in 0.1 M phosphate buffer, pH 7.2. After rinsing in water and dehydration in acetone, the fixed mycelia were stained in 2% uranyl acetate in acetone for 2 hours at 4°C in a darkroom. Specimens were then embedded in Araldite resin. Ultrathin sections were contrasted with lead citrate and examined in a Philips Tecnai 12 Biotwin (120 kV).

Results

Truncated HET-s(157-289) protein displays [Het-s]-incompatibility function

We have previously reported that the HET-s PFD (residues 218-289) fused to GFP allows [Het-s] prion propagation but does not display wild-type incompatibility function (Balguerie et al., 2003) (Fig. 1A). Macroscopically, the incompatible interaction between *het-s* and *het-S* alleles leads to the formation of a barrage when strains are confronted on solid medium and undergo cell fusion. A strain expressing HET-s(218-289)/GFP displays only an attenuated incompatibility reaction when confronted to a [Het-S] tester and a strain expressing just the HET-s(218-289) peptide shows no barrage reaction at all (Fig. 1B). The HET-s PFD is necessary but not sufficient for the incompatibility function. This indicates that sequences upstream of the PFD are required for full incompatibility function. We thus asked whether a truncated form of HET-s retaining part of the sequence corresponding to the globular domain could display normal incompatibility function. A vector designated pGPD-het-s(157-289) allowing the expression of roughly the C-terminal half of the HET-s protein (residues 157-289) was constructed and introduced into a *Δhet-s* strain. Transformants were confronted to a [Het-s] strain and then analysed for their ability to propagate [Het-s] and for the incompatibility function. Transformants expression HET-s(157-289) were able to propagate [Het-s] and to produce a normal barrage reaction when confronted to a [Het-S] tester (Fig. 1B).

To confirm that HET-s(157-289) is active in incompatibility, we introduced the pGPD-het-s(157-289) vector into a *het-S* background. If HET-s(157-289) is active in incompatibility, such transformants should grow very poorly. We found, as expected, that transformants expressing HET-s(157-289) in a *het-S* background are drastically affected in their growth. Radial growth rate on solid medium was strongly reduced (Fig. 1C). Hyphae displayed extensive vacuolization, a cytological manifestation characteristic of the incompatibility reaction (Dementhon et al., 2003) (Fig. 1D). By contrast, the pGPD-het-s(157-289) transformants of *het-s* or *Δhet-s* strains grew as the wild type (Fig. 1C). These results further confirm that HET-s(157-289) displays [Het-s]-incompatibility activity.

Together, these experiments indicate that the HET-s(157-289) protein can be converted to the infectious prion state and retains the [Het-s]-incompatibility function.

Recombinant HET-s(157-289) is converted to amyloid fibers in vitro

In order to investigate the structural properties of this functional truncated version of the HET-s prion protein, we expressed this protein in *Escherichia coli* with a C-terminal histidine tag. The HET-s(157-289) protein was purified from inclusion bodies under denaturing conditions. Upon exchange of the 8 M urea buffer for a non-denaturing buffer, the protein was initially soluble but formed aggregates over time (Fig. 2A). At 20°C without agitation and at a concentration of 0.2 mg ml^{-1}, half of the protein was aggregated after about 10 hours. The aggregation rate of HET-s(157-289) is thus considerably higher than that of full-length HET-s and is comparable to that of the HET-s(218-289) prion domain alone (Dos Reis et al., 2002; Balguerie et al., 2003). We then determined whether

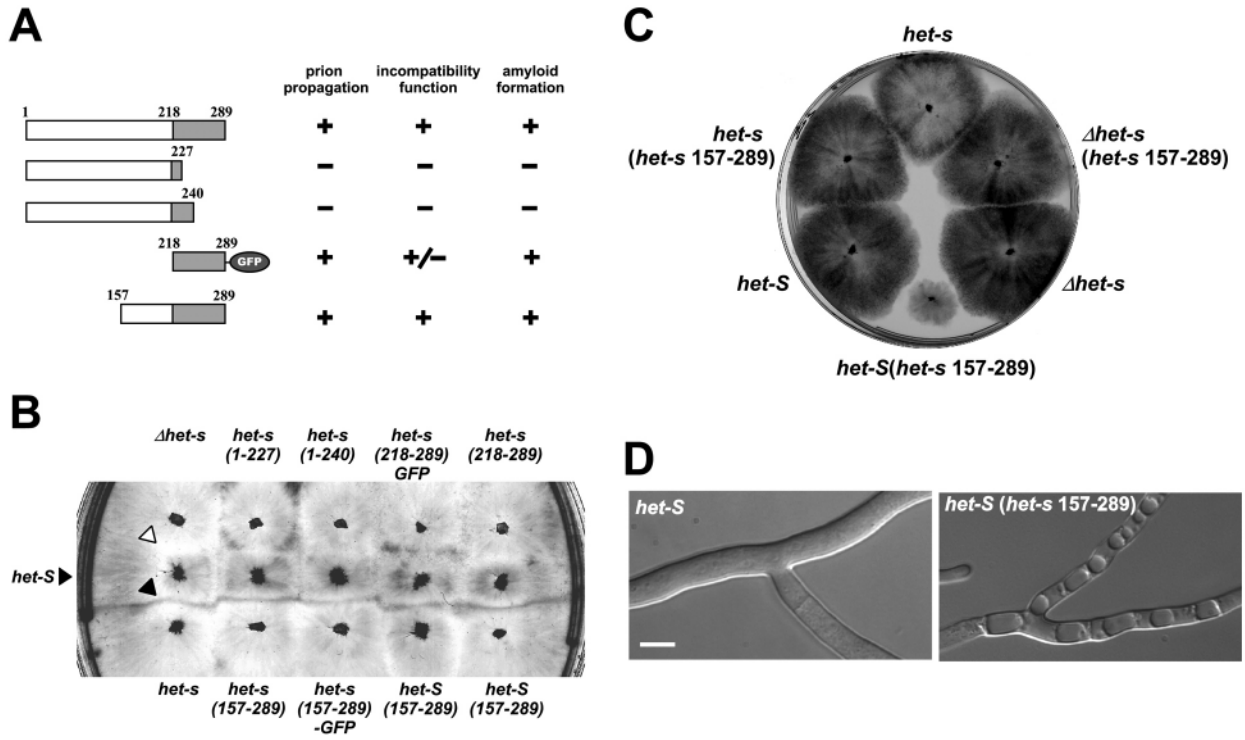

Fig. 1. Activity of HET-s deletion constructs. (A) On the left, various deletion constructs of HET-s are depicted. Numberings correspond to amino acid positions. The prion-forming domain is shown in gray. For each construct, the abilities to propagate [Het-s], to produce a barrage reaction toward *het-S* (incompatibility function) and to aggregate into amyloid fibrils in vitro are listed. For the 218-289 construct, the results are for the 218-289 peptide fused to GFP. (B) Barrage test with various HET-s deletion constructs: a *het-S* tester strain (central line) was confronted on solid medium with strains bearing various HET-s deletion constructs. Confrontation between incompatible strains leads to the formation of a dark, dense contact line termed the barrage (black, arrowed). Compatible strains display normal clear contact lines (white arrowed). The strains that do not produce a barrage reaction to *het-S* are grouped on the top line; the strains producing a barrage reaction to *het-S* are on the bottom line. Notice the attenuated barrage reaction obtained with the *het-s(218-289)GFP* construct. (C) Strains were cultivated for 5 days on solid medium. Notice that expression of HET-s(157-289) in a *het-S* background strongly affects growth, whereas strains expressing HET-s(157-289) in a *het-s* or *Δhet-s* background display normal growth. (D) Microscopic examination of a transformant expressing HET-s(157-289) in a *het-S* background and of an untransformed *het-S* control strain. Notice the extensive vacuolization of the hyphae in strains expressing HET-s(157-289). Scale bar, 4 μm.

aggregates of HET-s(157-289) can catalyse aggregation of the full-length HET-s protein. After inoculation with an aliquot of aggregated HET-s(157-289), full-length HET-s aggregation was complete after just a few hours (Fig. 2A). By comparison, spontaneous aggregation of the same full-length HET-s sample mock inoculated with buffer alone took more than 48 hours, indicating that HET-s(157-289) aggregates can catalyse aggregation of full-length HET-s.

In order to gain information on the secondary structure content of the soluble and aggregated forms of HET-s(157-289), we have recorded the far-ultraviolet CD spectra of the protein under both conditions. The CD spectra of the soluble and aggregated forms differ greatly, indicating that the protein undergoes a substantial structural rearrangement upon aggregation (Fig. 2B). The CD spectrum of the soluble form displays a minimum at 198 nm, suggesting a high content in random coil structures. The spectrum of the aggregated form displays a minimum around 218 nm and a positive signal around 196 nm, suggesting an increase in β-sheet secondary structures.

When observed by electron microscopy, HET-s(157-289) aggregates appeared as typical amyloid fibers (Fig. 3). Fibers were often more than 30 μm long and of variable width (~15-100 nm) (Fig. 3A). Such fibers are formed of bundles of individual fibrils ~2 nm wide that associate laterally (Fig. 3B-D). The bundles separate into individual fibrils (Fig. 3C,D). These fibers were large enough to be observed by conventional light microscopy (Fig. 3E) or fluorescence microscopy after staining with Congo red (Fig. 3F).

We conclude from these analyses that recombinant HET-s(157-289) undergoes a transition from a soluble to an aggregated amyloid state in vitro.

Proteinase-K-resistant amyloid core of HET-s(157-289) and full-length HET-s aggregates

Limited proteolysis has been used to gain insight into the process of amyloid formation (Kheterpal et al., 2001; Polverino de Laureto et al., 2003; Baxa et al., 2003). We have previously defined the proteinase-K-resistant amyloid core of full-length HET-s aggregates as a peptide spanning residues 218-289 (Balguerie et al., 2003). In order to delineate the amyloid core of HET-s(157-289) aggregates, we submitted HET-s(157-289) to limited proteolysis (Fig. 2C). Soluble HET-s(157-289) was rapidly degraded and produced a pattern with three discrete bands only visible for very short digestion times. Digestion of

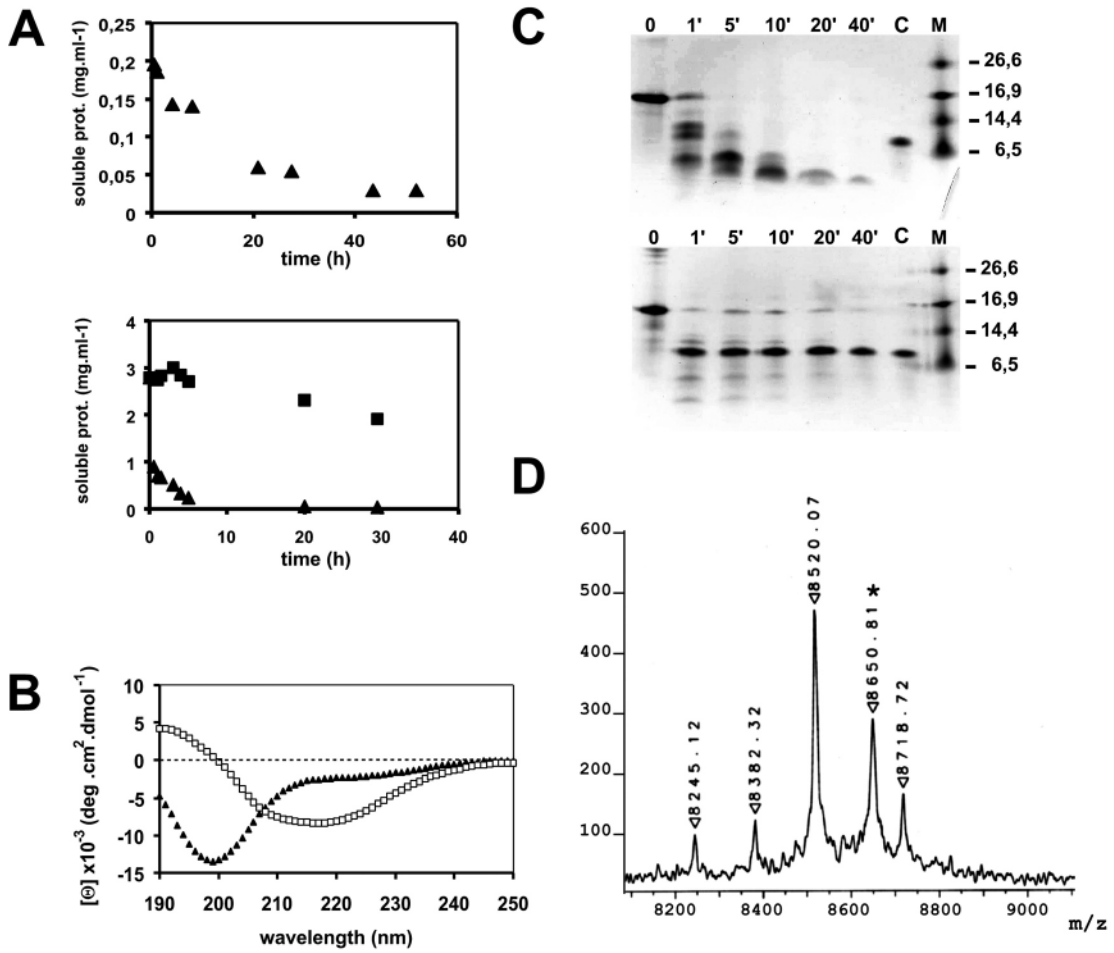

Fig. 2. Aggregation and formation of a proteinase-K-resistant core in recombinant HET-s(157-289). (A) Recombinant HET-s(157-289) aggregates in vitro and catalyses the aggregation of full-length HET-s. (top) Time course of aggregation at 0.2 mg ml^{-1} at 20°C. (bottom) Aggregation of recombinant full-length HET-s protein at 3 mg ml^{-1} inoculated with an aliquot (0.1 mg ml^{-1}) of aggregated HET-s(157-289) (triangles) or buffer alone (squares). (B) Circular dichroism spectra of 20 μM recombinant HET-s(157-289) at pH 8 in the soluble (black triangles) and aggregated (white squares) states. (C) Time course of limited proteinase-K digestion of soluble (top) and aggregated (bottom) recombinant HET-s(157-289) protein analysed by SDS-PAGE followed by Coomassie-Blue staining. Digestion times are given in minutes. The last lane (218-289) corresponds to the recombinant HET-s(218-289) peptide. Size of molecular weight markers (M lane) is given in kDa. (D) Mass spectrum of the proteinase-K-resistant material. The *y* axis gives intensity in arbitrary units, the *x* axis gives mass-to-charge (*m*/*z*) ratios in Daltons per unit charge. The peak at 8650.81 Da (*) corresponds to an internal control (recombinant 218-289 peptide with a six-histidine extension). The major peak at 8520.07 was identified as the 218-289 fragment (with six histidines). The 130.74 Da difference in the measured average mass between the control recombinant 218-289 peptide (*) and the major peak is caused by the recombinant peptide displaying an additional N-terminal methionine residue (theoretical mass difference 131.20 Da).

aggregated HET-s(157-289) produced a radically different pattern characterized by a single major digestion product of about 8 kDa. This fragment had the same electrophoretic mobility as the histidine-tagged HET-s(218-289) peptide used as a control (Fig. 2C). The resistant fragment was found to bind nickel nitrilotriacetic acid horseradish peroxidase (Ni-NTA HRP) conjugate in western-blot experiments (data not shown), indicating that it retains the C-terminal histidine tag of HET-s(157-289). Together, these experiments suggest that the amyloid core of HET-s(157-289) encompasses the same region as in full-length HET-s amyloids (residues 218-289). In order to characterize this proteinase-K-resistant material precisely, we analysed the HET-s(157-289) digestion products by mass spectrometry.

This analysis revealed a major species at 8520.07 Da (average mass). This major peak was unambiguously identified as the 218-289 fragment with the six-histidine extension (theoretical average mass of 8520.44 Da). Two minor peaks of smaller mass at 8382.32 Da and 8245.12 Da (average masses) matched the expected mass for a 218-289 fragment lacking respectively one or two C-terminal histidines (respective theoretical average masses of 8383.32 Da and 8246.16 Da). A third minor peak of higher mass at 8718.72 Da matched the expected mass for the 216-289 fragment with six histidines (theoretical average mass of 8719.65 Da). To assess the accuracy of average mass measurements, we used an internal standard corresponding to the recombinant 218-289 peptide (with a six-histidine extension and an N-terminal methionine residue), which was mixed with the proteolysis products. The measured average mass for this peptide was 8650.81 Da for a

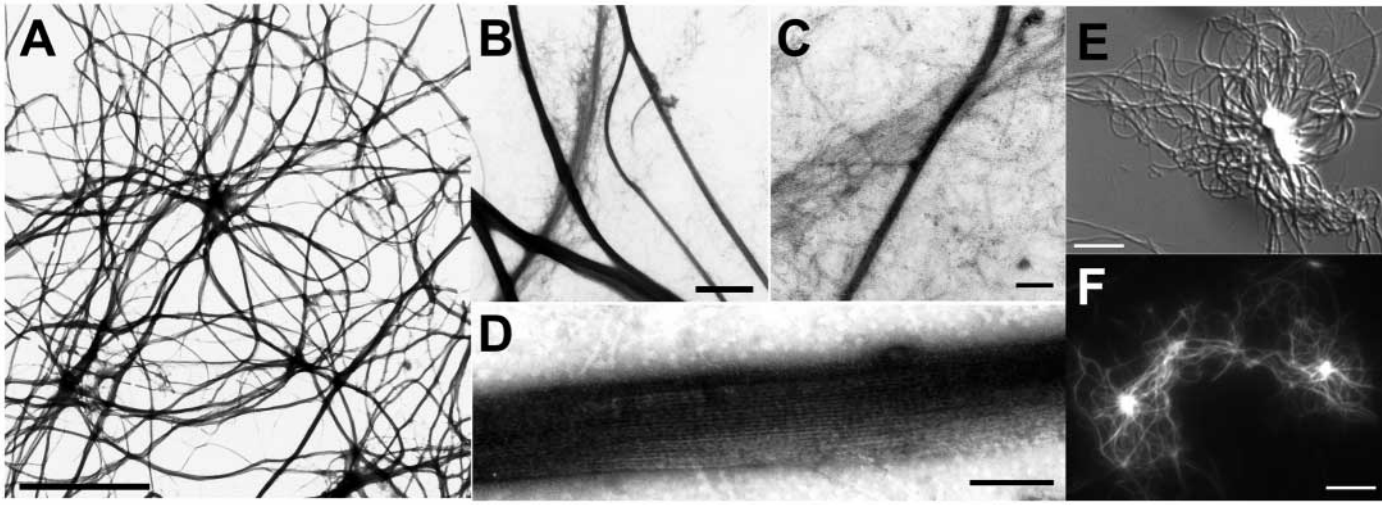

Fig. 3. Amyloid fibrils of recombinant HET-s(157-289). (A-D) Electron microscopy of HET-s(157-289) aggregates. (B,C) Tightly compacted fibrils and more loosely organized bundles fringing out into individual fibrils. (D) The well-ordered lateral association of individual fibrils. Scale bars, 10 μm (A), 500 nm (B), 200 nm (C), 100 nm (D). (E) light microscopy of HET-s(157-289) fibrils. Scale bar, 10 μm. (F) Fluorescence microscopy of HET-s(157-289) stained with Congo red. Scale bar, 10 μm.

theoretical average mass of 8651.63. This indicated an accuracy of about ±1 Da in average mass measurements. Together these experiments are fully consistent with the SDS-PAGE characterization of the proteinase-K-resistant material and confirm that the resistant region corresponds to the 218-289 fragment although a minor product spanning residues 216-289 could also be detected.

We conclude that upon aggregation of HET-s(157-289) a proteinase-K-resistant amyloid core is formed. This amyloid core encompasses the same region as in full-length HET-s amyloids, namely residues 218-289.

HET-s(157-289)/GFP forms elongated aggregates in vivo

In order to study HET-s(157-289) aggregation in vivo, a vector allowing the expression of a C-terminal HET-s(157-289)/GFP fusion protein was constructed and introduced in into a *Δhet-s* recipient. Strains expressing HET-s(157-289)/GFP were found to exist under two distinct phenotypes. They were either neutral in incompatibility and unable to induce the [Het-s*] to [Het-s] transition ([Het-s*] phenotype) or active in incompatibility and able to propagate [Het-s] ([Het-s] phenotype). In *het-s(157-289)/GFP* [Het-s*] strains, the fluorescence was diffuse and cytoplasmic (Fig. 4A). Conversely, in *het-s(157-289)/GFP* [Het-s] strains, the GFP signal corresponded to cytoplasmic aggregates (Fig. 4B). When [Het-s*] *het-s(157-289)/GFP* strains displaying diffuse GFP were infected with [Het-s] (i.e. confronted with a [Het-s] strain), the transformants turned to the [Het-s] phenotype and the HET-s(157-289)/GFP fusion protein formed aggregates. Transition to the [Het-s] phenotype also occurred spontaneously when cultures aged or during subculturing. We concluded that addition of the GFP tag did not alter the activity of HET-s(157-289) in prion propagation and incompatibility function.

In contrast to full-length HET-s/GFP or HET-s(218-289)/GFP fusion proteins which produce small dot-like aggregates (Coustou-Linares et al., 2001; Balguerie et al., 2003), HET-s(157-289)/GFP formed elongated aggregates. HET-s(157-289)/GFP aggregates often reached considerable sizes (more than 150 μm long) (Fig. 4C). The longest aggregates were systematically found in the apical region of the hyphae. In this region, the hyphae are not septated and this presumably allows aggregates to become very long. By contrast, in mature septated hyphae, fibril extension was often blocked by the septa (Fig. 4D). In the apical regions, fibril did not extent to the very tip of the filament (Fig. 4C). In the apex, the cytoskeleton is known to be highly organized in order to allow polarized tip growth (Geitmann et al., 2000). It is possible that this cytoskeletal structure prevents fibril elongation into that region. In most filaments, the elongated aggregates are straight but they were not totally rigid because they were capable of bending (Fig. 4D-G). This occurred in particular when they are submitted to a mechanical constraint, for instance when blocked by a septum (Fig. 4D), when growing in a lateral hyphal branch (Fig. 4F) or extending through an anastomosis bridge (Fig. 4G). Elongated aggregates were also readily detected in microconidia (male reproductive cells) (Fig. 4H).

Time-lapse microscopy analyses were performed to study fibril dynamics. Fibrils moved freely within the filaments, apparently as a consequence of intrahyphal cytoplasmic flow [Fig. 5; see supplementary movie 1 (http://jcs.biologists.org/supplemental/)]. It appears that aggregates grow by the lateral association of fibrils that become entangled to form larger ones. The sequence in Fig. 6 illustrates this process (see also supplementary movies 2, 3). Fibrils have a strong tendency to self-associate, which readily explains why in most fungal ‘cells’ (delimited by two septa) only a single, very large aggregate is found. Thinner fibrillar aggregates are also occasionally observed (see supplementary movie 1).

The elongated aggregates could deteriorate in various ways. Upon prolonged exposure to ultraviolet light during microscopy or in aging hyphae, elongated aggregates sometimes collapsed or retracted into curly structures (Fig.

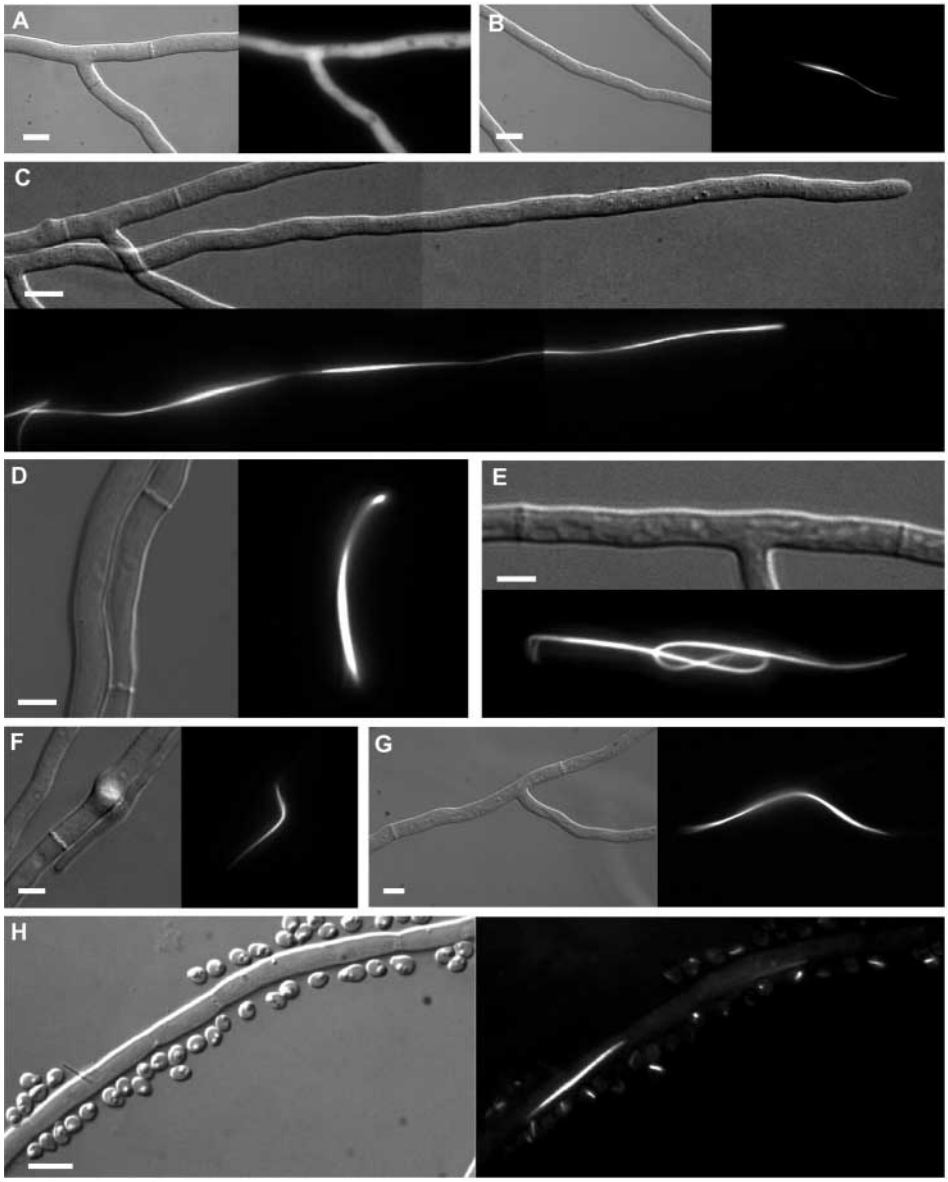

Fig. 4. HET-s(157-289)/GFP forms elongated fibrillar aggregates in vivo upon transition to the prion state. (A) Strains expressing HET-s(157-289)/GFP were analysed by fluorescence microscopy. In the [Het-s*] state, the fluorescence signal is diffuse and cytoplasmic. (B) Upon transition to the [Het-s] prion state, HET-s(157-289) forms fibrillar aggregates. (C) In apical regions, in which septa are absent, fibrillar aggregates grow very large. (D,E) Aggregates are not rigid and are able to bend when blocked by septa. (F) Aggregates are able to pass through an anastomosis bridge. (G) Aggregate extending into an hyphal branch. (H) HET-s(157-289) are incorporated into microconidia. Scale bar, 4 μm.

7A; see supplementary movies 4, 5 (http://jcs.biologists.org/supplemental/). Also, the fibrils appeared to get peeled apart or deteriorated when passing through septal pores (Fig. 7B; see supplementary movie 6). Finally, when cellular integrity was disrupted by mechanical or osmotic cell lysis, the aggregates maintained their fibrillar state but dispersed into smaller fibrils (Fig. 7C). This also occurred in cells undergoing cell death (data not shown). This suggests that cellular integrity is required to maintain these large elongated aggregates.

Strains expressing HET-s(157-289)/GFP in its aggregated form were also analysed by electron microscopy. Such strains were found to contain cytoplasmic fibrillar structures about 200 nm wide formed by the lateral association of individual fibers with an estimated width of about 20 nm (Fig. 8). Such structures were not observed in untransformed control strains (not shown).

We conclude from these observations that the HET-s(157-289) protein is able to form highly ordered elongated structures in vivo that are composed of lateral association of smaller fibrillar aggregates. This organization is unique to HET-s(157-289), because both full-length-HET-s/GFP and HET-s(218-289)/GFP form only dot-like aggregates in vivo (Coustou-Linares et al., 2001; Dos Reis et al., 2002).

Full-length HET-s and HET-s(218-289) form elongated aggregates when expressed with HET-s(157-289)

Full-length HET-s and HET-s(157-289) form aggregates of distinct high-order organization in vivo (dots versus elongated structures). We have shown above that HET-s(157-289) can seed the aggregation of full-length HET-s in vitro, suggesting that HET-s and HET-s(157-289) can co-aggregate. This prompted us to analyse the effect of co-expression of HET-s and HET-s(157-289) on aggregate organization in vivo. To that end, we have transformed a *Δhet-s* strain with a vector driving expression of HET-s/GFP and also with a vector driving expression of untagged HET-s(157-289). In both vectors, expression is driven by the same promoter. In such co-

transformants, the HET-s/GFP fluorescence was detected as elongated aggregates (Fig. 9). In addition, dot-like aggregates were also observed that were sometimes associated with the elongated aggregates. This experiment indicates that full-length HET-s can organize into ordered elongated fibrillar aggregates when expressed with HET-s(157-289). The fact that full-length HET-s/GFP is detected as fibrillar elongated aggregates strongly suggests that HET-s/GFP and HET-s(157-289) co-aggregate in vivo. The fluorescence signal of the observed elongated aggregates was comparable to that

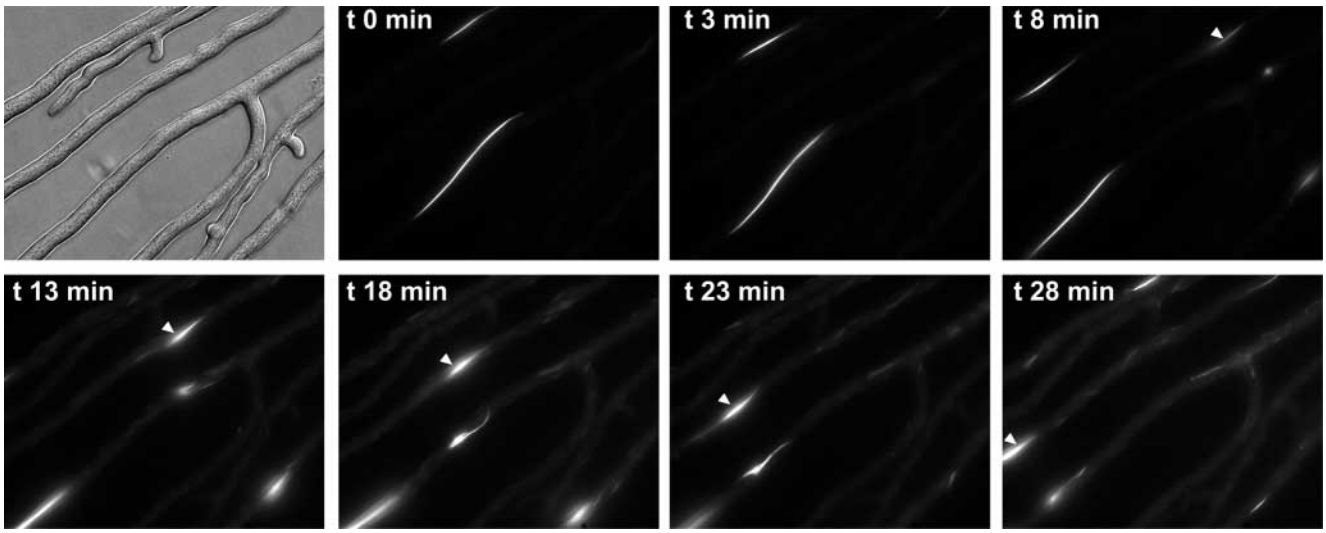

Fig. 5. Intracytoplasmic movement of HET-s(157-289)/GFP aggregates. (Triangle) A HET-s(157-289)/GFP aggregate as it moves within the filament through the analysed field. Notice the absence of septa in the analysed region. The sequence is taken from supplementary movie 1 (http://jcs.biologists.org/supplemental/).

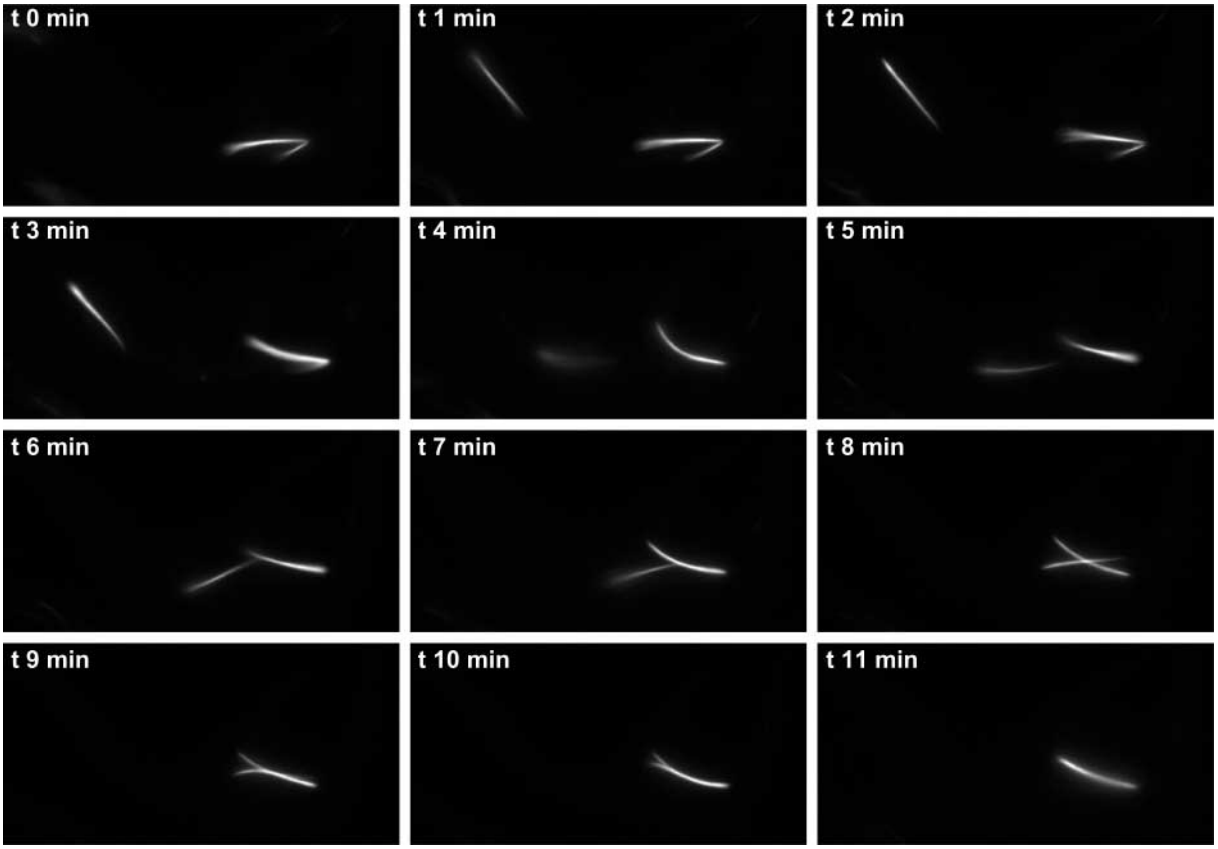

Fig. 6. Association of HET-s(157-289)/GFP aggregates. Notice the coalescence of the aggregates into a single fibrillar aggregate once at 4 minutes and again at 11 minutes. The sequence is taken from supplementary movie 2 (http://jcs.biologists.org/supplemental/) (see also supplementary movie 3).

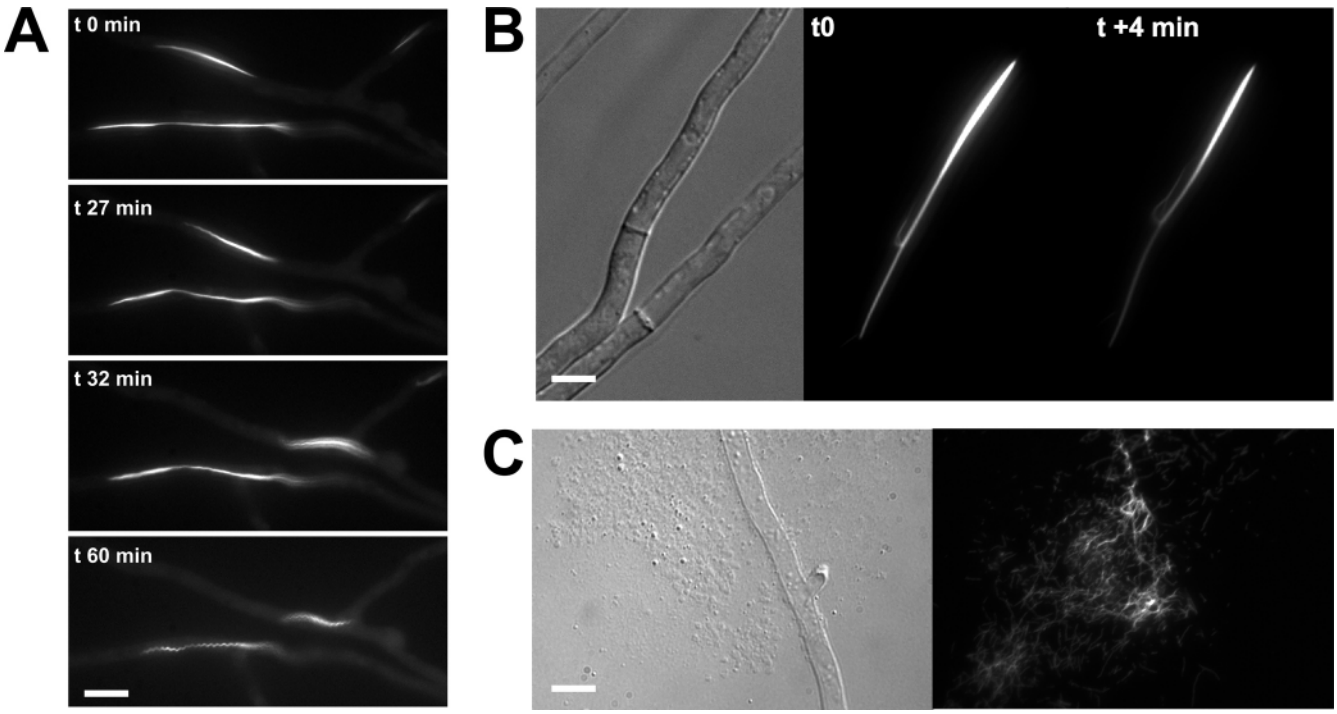

Fig. 7. Deterioration of HET-s(157-289)/GFP aggregates. (A) HET-s(157-289) aggregates retract into curly structures upon aging. The sequence is taken from supplementary movie 4 (http://jcs.biologists.org/supplemental/) (see also supplementary movies 5, 6). (B) Fibril deterioration as an aggregate passes through a septal pore. (C) Upon hyphal lysis, aggregates dissociated into many smaller fibrils. Scale bar, 4 μm.

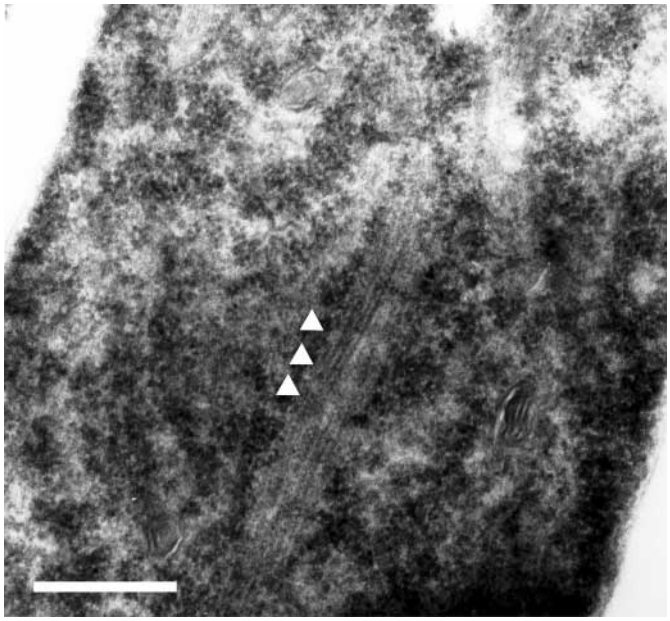

Fig. 8. HET-s(157-289) aggregates formed in vivo observed by electron microscopy. HET-s(157-289) aggregates are marked by arrowheads. Scale bar, 500 nm.

observed using HET-s(157-289)/GFP, suggesting that the aggregates contain a significant proportion of full-length HET-s. In the reciprocal transformation experiments using HET-s and HET-s(157-289)/GFP, elongated aggregates were also detected (data not shown).

We then performed the same experiment using the HET-s PFD (residues 218-289) tagged with GFP. When expressed alone, HET-s(218-289) forms only dot-like aggregates (Fig. 9) (Balguerie et al., 2003) but, when HET-s(218-289)/GFP was expressed with HET-s(157-289), elongated aggregates were observed. Elongated aggregates co-existed with dot-like aggregates. Again, as in the case of full-length HET-s, HET-s(157-289) is able to modify the higher order organization of HET-s(218-289)/GFP.

We conclude that the ability to organize into large, elongated fibrillar aggregates is a specific feature of HET-s(157-289) and that this truncated protein is able to impose this higher-order organization on both full-length HET-s and HET-s(218-289).

Deletion in the globular domain of HET-S leads to a specificity switch to the [Het-s] phenotype

We decided to determine the effect a deletion of the N-terminal region on the activity of the HET-S protein. Vectors allowing the expression of HET-S(157-289) and HET-S(157-289)/GFP proteins were constructed and introduced into a Δ*het-s* recipient strain. HET-S(157-289) differs from HET-s(157-289) by five residues (positions 165, 186, 235, 253 and 274). Transformants expressing HET-S(157-289) or HET-S(157-289)/GFP lacked the [Het-S] phenotype and did not produce a barrage reaction toward [Het-s] strains. Instead, they displayed the [Het-s] phenotype. They were able to propagate [Het-s] and produced an incompatibility reaction when confronted with a [Het-S] tester (Fig. 1B).

In HET-S(157-289)/GFP transformants expressing the [Het-s*] phenotype, fluorescence was diffuse and cytoplasmic,

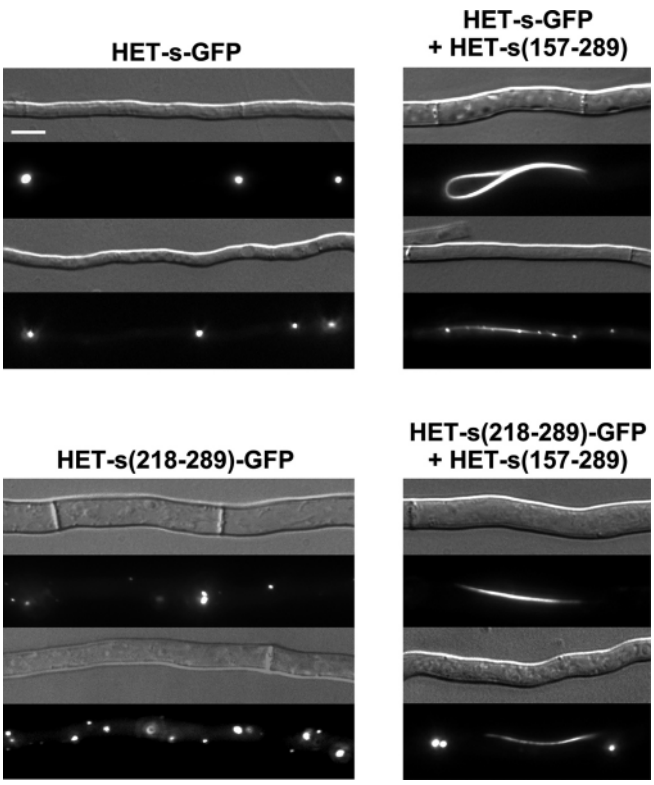

Fig. 9. HET-s/GFP and HET-s(218-289)/GFP form elongated fibrillar aggregates when expressed with HET-s(157-289). In the prion state, HET-s/GFP and HET-s(218-289)/GFP form dot-like aggregates when expressed alone (left) but fibrillar aggregates when expressed with HET-s(157-289) (right). Notice that dot-like aggregates co-exist with fibrillar aggregates in strains expressing either HET-s/GFP and HET-s(157-289) or HET-s(218-289)/GFP and HET-s(157-289). Scale bar, 4 μm.

whereas fluorescence appeared as aggregates in HET-S(157-289)/GFP transformants of the [Het-s] phenotype (Fig. 10). Like HET-s(157-289)/GFP, HET-S(157-289)/GFP organized into elongated fibrillar aggregates that were often not as regular as those observed with HET-s(157-289)/GFP (Fig. 10). For instance, in various aggregates, the width appeared to be variable along the aggregate. Also, at the extremity of the very long aggregates typical of the apical region, aggregates became curly and disorganized, and circular ring-shaped aggregates were often detected (Fig. 10). Such structures were not observed with HET-s(157-289)/GFP.

We conclude from this experiment that a deletion in the N-terminal region in HET-S leads to a specificity switch to the [Het-s] incompatibility type. In addition, we conclude that the five amino-acid differences between HET-s(157-289) and HET-S(157-289) are responsible for modest but significant differences in higher-order aggregate organization.

Discussion

HET-s(157-289) aggregates are not toxic per se

Here, we have shown that the HET-s prion protein of the fungus *P. anserina* truncated of its N-terminal 156 residues still displays activity in terms of both prion propagation and heterokaryon incompatibility. In vivo, this truncated version of HET-s forms elongated aggregates. Such fibrillar aggregates formed in vivo by fungal prion proteins have been reported previously. In yeast, the Ure2p protein was found to form a fibrillar network in the cytoplasm (Speransky et al., 2001). Formation of elongated and ring-like Sup35p-GFP aggregates has also been reported (Zhou et al., 2001). However, here, owing to the particular cellular organization of filamentous fungi, growth of such elongated fibrillar structures is not restricted to a single cell as it is in yeast. The aggregates observed in *Podospora* can thus grow to considerable sizes. These structures grow by lateral association of shorter fibrillar aggregates. Considering that the HET-s(157-289) protein forms amyloids in vitro, it is reasonable to assume that these aggregates are composed of amyloid or amyloid-like structures. Several human neurodegenerative disorders are characterized by accumulation of amyloid aggregates in the brain. It is, however, becoming increasingly clear that the large amyloid aggregates themselves are not the neurotoxic species in these diseases (Bucciantini et al., 2002; Caughey and Lansbury, 2003). Consistent with this current view on amyloid toxicity is the fact that strains containing large amounts of HET-s(157-289) aggregates showed normal growth rates and viability. The present study indicates that massive intracytoplasmic accumulation of large amyloid-like aggregates in *Podospora* does not affect cell viability to a significant extend. HET-s(157-289) only becomes toxic when expressed with HET-S.

HET-s(157-289) fibril organization in vitro

Current models of the structure of filaments of the fungal prion proteins propose the existence of a central amyloid core in a β-sheet structure surrounded by globular portions in a native or near-native fold. This view is supported by strong experimental evidence in the case of Ure2p (Baxa et al., 2003). The available data on HET-s fibril architecture are also fully consistent with this model (Balguerie et al., 2003; Nazabal et al., 2003). The extensive deletion in the N-terminal globular domain in HET-s(157-289) is likely to prevent proper folding of this region and, indeed, the CD spectrum of soluble HET-s(157-289) suggests that this peptide is poorly structured. It was therefore conceivable that additional unfolded regions might be incorporated into the amyloid core of the fiber, but this appears not to be the case. The amyloid core of HET-s(157-289) is the same as that of full-length HET-s, suggesting that the region from 157 to 218 is not competent to adopt the amyloid fold. In the amyloid core model, the 157-218 region protrudes from the amyloid core in HET-s(157-289) fibrils. We have previously reported that, in electron microscopy, full-length HET-s fibrils appear twisted and ‘ropey’, whereas HET-s(218-289) fibrils (which contain only the PFD) are smooth (Balguerie et al., 2003). This difference was attributed to the fact that, in full-length HET-s fibrils, the globular domain protruding from the amyloid core imposes spatial constraints on fibrils organization. We find here that HET-s(157-289) fibrils are also smooth, which suggests that the short portion of the globular domain decorating the amyloid core in HET-s(157-289) aggregates does not impose a significant constraint on fibrils organization in vitro.

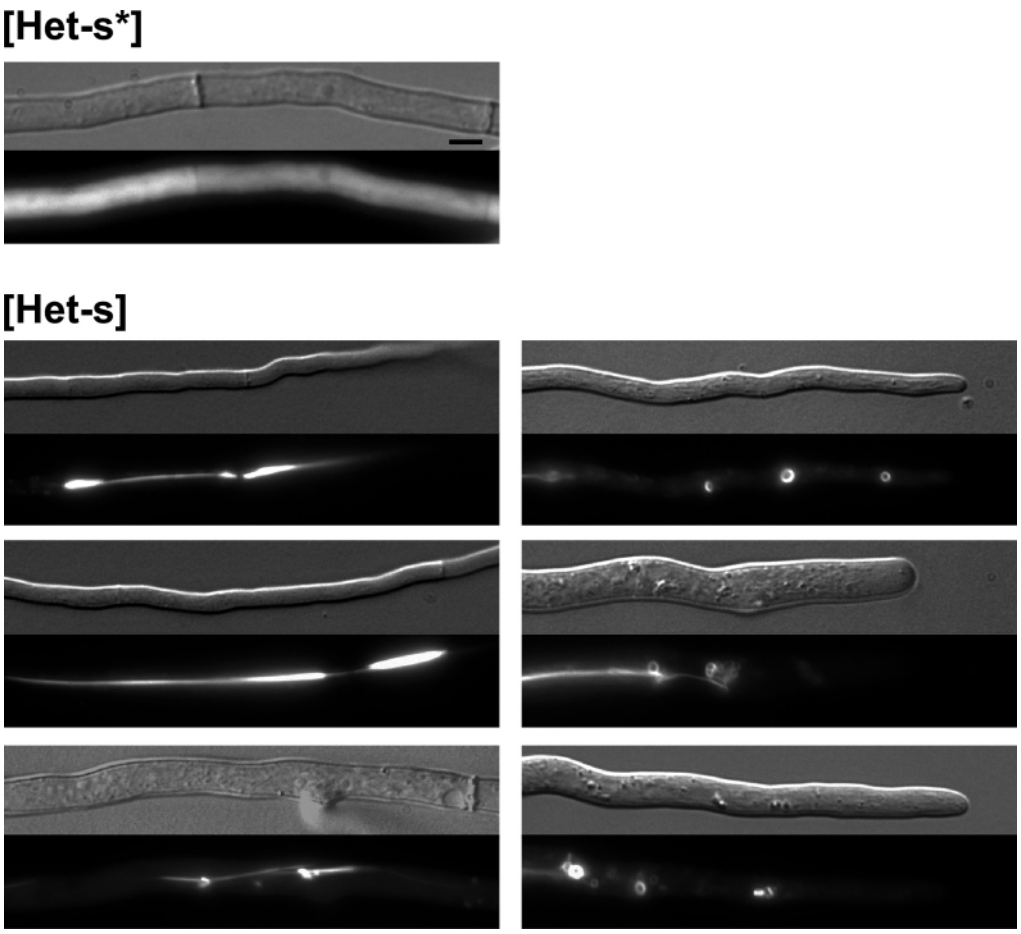

Fig. 10. HET-S(157-289)/GFP aggregates upon transition to the [Het-s] state. Upon transition to the [Het-s] prion state, HET-S(157-289)/GFP forms fibrillar aggregates. Notice that fibrillar aggregates are often not as regular as HET-s(157-289)/GFP aggregates (left). In apical regions (right), donut-shaped circular structures are detected. Scale bar, 2 μm.

Supramolecular organization of HET-s(157-289) aggregates in vivo

We find that HET-s(157-289) forms very large elongated aggregates in vivo. In contrast to HET-s(157-289), full-length HET-s-GFP and HET-s(218-289) do not reach that level of supramolecular organization and instead coalesce into discrete dot-like structures (Coustou-Linares et al., 2001). Still, even these dot-like aggregates are likely to be composed of amyloid or amyloid-like fibrils, because full-length HET-s aggregates formed in vivo were found to induce amyloid polymerization of recombinant HET-s in vitro (Maddelein et al., 2002). Our time-lapse-microscopy experiments suggest that HET-s(157-289) aggregates have a strong tendency to stick together and to associate laterally. It appears that the HET-s(157-289) construct specifically promotes such lateral associations between short fibrils to form very long bundles. This lateral association presumably involves the 157-218 region protruding from the amyloid core. It is possible that hydrophobic stretches of the 157-218 region that are normally buried within the protein are exposed in the fibrils and cause the fibrils to self-associate laterally. The large, elongated organized structures formed by HET-s(157-289) are not maintained in damaged cells, raising the possibility that the cellular machinery is required for their build up and maintenance.

It has been previously reported that the nature of the sequence attended to the PFD can affect amyloid morphology of the Ure2p, Sup35p and HET-s fungal prion proteins in vitro (Glover et al., 1997; Baxa et al., 2002; Balguerie et al., 2003; Baxa et al., 2003). Our data now clearly indicate that the nature of the N-terminal sequence appended to the PFD of HET-s strongly affects the supramolecular organization of the prion protein aggregates in vivo. Subtle amino acid differences such as those existing between HET-s(157-289) and HET-S(157-289) can also influence aggregate morphology in vivo. In particular, circular aggregates were obtained with HET-S(157-289) but not with HET-s(157-289).

How are the [Het-s] and [Het-S] incompatibility types specified?

It has been shown previously that the [Het-s] and [Het-S] incompatibility types are defined by the polymorphisms at two discrete amino acid positions in the N-terminal globular domain (residues 23 and 33) (Deleu et al., 1993). We report here that most of the region corresponding to the N-terminal globular domain (encompassing these polymorphic positions) is dispensable for the [Het-s] incompatibility function. In addition, deletion of this same region in HET-S leads to a specificity switch to the [Het-s] incompatibility type. The present observations are not consistent with a simple model in which the N-terminal regions of HET-s and HET-S are involved in a protein-protein interaction process allowing specific recognition between either similar or unlike *het* gene products. Instead, integrity of the globular domain appears to be required

to specify the [Het-S] incompatibility type, whereas alterations of this domain by deletion or mutation lead to expression of the [Het-s] incompatibility type. The mechanism that causes death in cells expressing both HET-s and HET-S remains largely elusive. Our current working hypothesis is based on the emerging models on amyloid toxicity in human disease (Bucciantini et al., 2002; Caughey and Lansbury, 2003). It is now generally believed that cell death in amyloid diseases is caused by oligomeric aggregation intermediates, whereas large 'mature' amyloids are harmless. These oligomeric species are thought to affect membrane integrity by forming pore-like structures. We have proposed that HET-S might inhibit the polymerization process of HET-s, leading to the accumulation of HET-s oligomers blocked in their polymerization process (Coustou-Linares et al., 2001). One possibility is that, once a HET-S monomer has been incorporated into a HET-s aggregate via its C-terminal PFD, the globular domain of HET-S hinders further polymerization. This model readily explains why the deletion in C-terminal PFD abolishes both [Het-s] and [Het-S] function (Balguerie et al., 2003), whereas a deletion in the globular domain affects only the [Het-S] function.

The present analysis provides novel insights into the mechanisms that govern higher-order prion protein aggregate organization in vivo. It also contributes our understanding of the way the HET-s prion triggers cell death when interacting with the antagonistic HET-S protein.

This work was supported by the GIS infections à prions. We thank Marc Blondel for critical reviewing of the manuscript.

References

Balguerie, A., Dos Reis, S., Ritter, C., Chaignepain, S., Coulary-Salin, B., Forge, V., Bathany, K., Lascu, I., Schmitter, J. M., Riek, R. et al. (2003). Domain organization and structure-function relationship of the HET-s prion protein of *Podospora anserina*. *EMBO J.* **22**, 2071-2081.

Baxa, U., Speransky, V., Steven, A. C. and Wickner, R. B. (2002). Mechanism of inactivation on prion conversion of the *Saccharomyces cerevisiae* Ure2 protein. *Proc. Natl. Acad. Sci. USA* **99**, 5253-5260.

Baxa, U., Taylor, K. L., Wall, J. S., Simon, M. N., Cheng, N., Wickner, R. B. and Steven, A. C. (2003). Architecture of Ure2p prion filaments: the N-terminal domains form a central core fiber. *J. Biol. Chem.* **278**, 43717-43727.

Beisson-Schecroun, J. (1962). Incompatibilité cellulaire et interactions nucléocytoplamsiques dans les phénomènes de barrage chez le *Podospora anserina*. *Ann. Genet.* **4**, 3-50.

Bergès, T. and Barreau, C. (1989). Heat-shock at elevated temperature improves transformation efficiency of protoplats from *Podospora anserina*. *J. Gen. Microbiol.* **135**, 601-604.

Bucciantini, M., Giannoni, E., Chiti, F., Baroni, F., Formigli, L., Zurdo, J., Taddei, N., Ramponi, G., Dobson, C. M. and Stefani, M. (2002). Inherent toxicity of aggregates implies a common mechanism for protein misfolding diseases. *Nature* **416**, 507-511.

Carrol, A. M., Sweigard, J. A. and Valent-Central, B. (1994). Improved vectors for selecting resistance to hygromycin. *Fungal Genet. Newslett.* **41**, 22.

Caughey, B. and Lansbury, P. T., Jr (2003). Protofibrils, pores, fibrils, and neurodegeneration: separating the responsible protein aggregates from the innocent bystanders. *Annu. Rev. Neurosci.* **26**, 267-298.

Chang, S. T. and Tanaka, K. (1970). Culturing and embedding of filamentous fungi for electron micrography in the plane of the filaments. *Stain. Technol.* **45**, 109-113.

Coustou, V., Deleu, C., Saupe, S. and Begueret, J. (1997). The protein product of the *het-s* heterokaryon incompatibility gene of the fungus *Podospora anserina* behaves as a prion analog. *Proc. Natl. Acad. Sci. USA* **94**, 9773-9778.

Coustou-Linares, V., Maddelein, M. L., Begueret, J. and Saupe, S. J. (2001). In vivo aggregation of the HET-s prion protein of the fungus *Podospora anserina*. *Mol. Microbiol.* **42**, 1325-1335.

Deleu, C., Clave, C. and Begueret, J. (1993). A single amino acid difference is sufficient to elicit vegetative incompatibility in the fungus *Podospora anserina*. *Genetics* **135**, 45-52.

Dementhon, K., Paoletti, M., Pinan-Lucarre, B., Loubradou-Bourges, N., Sabourin, M., Saupe, S. J. and Clave, C. (2003). Rapamycin mimics the incompatibility reaction in the fungus *Podospora anserina*. *Eukaryot. Cell* **2**, 238-246.

Dos Reis, S., Coulary-Salin, B., Forge, V., Lascu, I., Begueret, J. and Saupe, S. J. (2002). The HET-s prion protein of the filamentous fungus *Podospora anserina* aggregates in vitro into amyloid-like fibrils. *J. Biol. Chem.* **277**, 5703-5706.

Glover, J. R., Kowal, A. S., Schirmer, E. C., Patino, M. M., Liu, J. J. and Lindquist, S. (1997). Self-seeded fibers formed by Sup35, the protein determinant of [PSI+], a heritable prion-like factor of *S. cerevisiae*. *Cell* **89**, 811-819.

Kheterpal, I., Williams, A., Murphy, C., Bledsoe, B. and Wetzel, R. (2001). Structural features of the Ab amyloid fibril elucidated by limited proteolysis. *Biochemistry* **40**, 11757-11767.

Maddelein, M. L., Dos Reis, S., Duvezin-Caubet, S., Coulary-Salin, B. and Saupe, S. J. (2002). Amyloid aggregates of the HET-s prion protein are infectious. *Proc. Natl. Acad. Sci. USA* **99**, 7402-7407.

Nazabal, A., Dos Reis, S., Bonneu, M., Saupe, S. J. and Schmitter, J. M. (2003). Conformational transition occurring upon amyloid aggregation of the HET-s prion protein of *Podospora anserina* analysed by hydrogen/deuterium exchange and mass spectrometry. *Biochemistry* **42**, 8852-8861.

Pinan-Lucarre, B., Paoletti, M., Dementhon, K., Coulary-Salin, B. and Clave, C. (2003). Autophagy is induced during cell death by incompatibility and is essential for differentiation in the filamentous fungus *Podospora anserina*. *Mol. Microbiol.* **47**, 321-333.

Polverino de Laureto, P., Taddei, N., Frare, E., Capanni, C., Costantini, S., Zurdo, J., Chiti, F., Dobson, C. M. and Fontana, A. (2003). Protein aggregation and amyloid fibril formation by an SH3 domain probed by limited proteolysis. *J. Mol. Biol.* **334**, 129-141.

Prusiner, S. B. (1982). Novel proteinaceous infectious particles cause scrapie. *Science* **216**, 136-144.

Prusiner, S. B. (1998). Prions. *Proc. Natl. Acad. Sci. USA* **95**, 13363-13383.

Punt, P. J., Dingemanse, M. A., Jacobs-Meijsing, B. J., Pouwels, P. H. and van den Hondel, C. A. (1988). Isolation and characterization of the glyceraldehyde-3-phosphate dehydrogenase gene of *Aspergillus nidulans*. *Gene* **69**, 49-57.

Rizet, G. (1952). Les phénomènes de barrage chez *Podospora anserina*. I. Analyse de barrage entre les souches s et S. *Rev. Cytol. Biol. Veg.* **13**, 51-92.

Speransky, V. V., Taylor, K. L., Edskes, H. K., Wickner, R. B. and Steven, A. C. (2001). Prion filament networks in [URE3] cells of *Saccharomyces cerevisiae*. *J. Cell Sci.* **153**, 1327-1336.

Taylor, J. P., Hardy, J. and Fischbeck, K. H. (2002). Toxic proteins in neurodegenerative disease. *Science* **296**, 1991-1995.

Turcq, B., Deleu, C., Denayrolles, M. and Begueret, J. (1991). Two allelic genes responsible for vegetative incompatibility in the fungus *Podospora anserina* are not essential for cell viability. *Mol. Gen. Genet.* **228**, 265-269.

Turcq, B., Denayrolles, M. and Bégueret, J. (1990). Isolation of two allelic incompatibility genes *s* and *S* of the fungus *Podospora anserina*. *Curr. Genet.* **17**, 297-303.

Zhou, P., Derkatch, I. L. and Liebman, S. W. (2001). The relationship between visible intracellular aggregates that appear after overexpression of Sup35 and the yeast prion-like elements [PSI+] and [PIN+]. *Mol. Microbiol.* **39**, 37-46.